Journal of Rock Mechanics and Geotechnical Engineering xxx (xxxx) xxx

Contents lists available at ScienceDirect

Journal of Rock Mechanics and Geotechnical Engineering

journal homepage: www.jrmge.cn

Full Length Article

Enhanced flexible pavement subgrade stability using activated carbon, coir fiber, and lime

Sakina Tamassoki [a,b], Shanyong Wang [a,*], Nik Norsyahariati Nik Daud [b,c,**], Mohammad Jawed Roshan [d]

[a] School of Engineering, The University of Newcastle, Callaghan, NSW, 2308, Australia
[b] Department of Civil Engineering, Faculty of Engineering, Universiti Putra Malaysia, Serdang, Selangor, 43400, Malaysia
[c] Housing Research Center, Faculty of Engineering, Universiti Putra Malaysia, Serdang, Selangor, 43400, Malaysia
[d] Department of Civil Engineering, ISISE, University of Minho, Campus de Azurim, Guimaraes, 4800-058, Portugal

ARTICLE INFO

Article history:
Received 21 November 2024
Received in revised form
8 May 2025
Accepted 10 June 2025
Available online xxx

Keywords:
Subgrade soil
Tensile strength
Finite element model (FEM)
Water level (WL)
Strain ratio

ABSTRACT

This study presents a method for improving flexible pavement subgrades using activated carbon and lime as stabilizers and coir fiber as reinforcement, improving subgrade performance using natural and recycled materials. Two residual soil types, Soil 1 and Soil 2, were examined for enhanced mechanical properties using California bearing ratio, indirect shear, direct shear, and consolidation tests. Pavement design calculations were performed using the empirical method, and finite element modeling was employed to assess the impact of water levels on subgrade settlement and strain ratios. The findings revealed notable improvements in cohesion and tensile strength when lime, activated carbon, and coir fiber were used for stabilization, achieving increases of up to 128.9 % and 167.71 % for Soil 1, and 155 % and 3045.86 % for Soil 2, respectively. Moreover, these stabilized samples exhibited the lowest penetration rates, recording values of 0.2 for both soils after 20 loading cycles. Incorporating a stabilized subgrade reduced the required subbase thickness by up to 90.91 % compared to the untreated condition. Finite element modeling indicated that the high-permeability Soil 1 sample experienced an average settlement of 70.12 mm under repeated loading, which is 2.46 times higher than the 28.54 mm observed in the low-permeability sample. Finally, strain ratio analysis confirmed that adding stabilizers effectively reduced the subgrade strain, bringing the strain ratio below one and thereby meeting the road subgrade standard. These findings highlight the innovative use of coir fiber, activated carbon, and lime as high-performance stabilizers for flexible pavement applications, offering a practical solution for infrastructure development.

1. Introduction

In civil engineering, soil stabilization and reinforcement techniques play crucial roles in enhancing the geotechnical properties of subgrade soil, ensuring pavement systems' longevity and structural integrity. Conventional stabilizers, such as lime and cement, have been widely used to improve soil properties (Roshan et al., 2024), including plasticity, density, shear strength, and durability (Behnood, 2018; Jairaj et al., 2020; Praveen and Kurre, 2021; Correia and Roshan, 2024). However, the increasing demand for sustainable alternatives has increased interest in natural and recycled materials (Hoy et al., 2023, 2024).

Lime stabilization effectively enhances soil strength (Tamassoki et al., 2023a), mitigates shrink-swell behavior, and reduces settlement. However, this may lead to brittleness, increasing the risk of structural failure under excessive loads (Abdi et al., 2021; Razali et al., 2023). Fiber reinforcement has been explored as an alternative to improve tensile strength (Farhangi et al., 2024) and transition soil behavior from brittle to ductile (Tiwari and Satyam, 2020). Coir fiber has shown promise in improving soil performance when

* Corresponding author.
** Corresponding author. Department of Civil Engineering, Faculty of Engineering, Universiti Putra Malaysia, Serdang, Selangor, 43400, Malaysia.
E-mail addresses: shanyong.wang@newcastle.edu.au (S. Wang), niknor@upm.edu.my (N.N.N. Daud).

Peer review under responsibility of Institute of Rock and Soil Mechanics, Chinese Academy of Sciences.

https://doi.org/10.1016/j.jrmge.2025.06.023

combined with lime, enhancing the California bearing ratio (CBR), shear strength, and tensile strength (Boobalan and Sivakami Devi, 2022) while reducing swell potential (Narendra Goud et al., 2018). In addition to lime and fiber reinforcements, activated carbon (AC) has emerged as a potential stabilizer because of its ability to enhance soil strength, reduce permeability, and adsorb CO_2 and contaminants (Lee et al., 2013; El-Shafey et al., 2016). Moreover, while producing 1 t of lime emits 0.86 t of CO_2, AC offers a more sustainable alternative by mitigating environmental impacts. Previous studies have demonstrated its effectiveness in improving the CBR, unconfined compressive strength (UCS), and shear resistance (Tiwari et al., 2021; Tamassoki et al., 2022a).

Given the importance of applicable and effective subgrade stabilization methods, understanding subgrade behavior under real-world conditions is challenging due to environmental variability and complex loading scenarios. Some studies have focused on the effects of cyclic loads on subgrade behavior, the use of geogrids to resist deformation, and the impact of flooding on pavement structural integrity (Chen et al., 2015; Tang et al., 2016; Arivalagan et al., 2022). Studies have also explored using binders, such as cement and lime, to improve subgrade strength, reduce swelling, and enhance pavement service life (Amakye et al., 2022). Additionally, numerical simulations and finite element model (FEM) have been employed to predict the subgrade behavior under varying conditions, such as fluctuating groundwater levels and different traffic loads (Elshaer and Daniel, 2018; Shojaeifard et al., 2020). Numerical models and simulations have significantly improved understanding of soil dynamics, moisture variations, and the effects of traffic loads on subgrade materials, highlighting factors such as cyclic loading, temperature changes, and slope stability (Li et al., 2022). Research has emphasized the importance of considering material composition, loading conditions, and environmental factors when assessing pavement durability. Innovations in modeling and laboratory testing have led to advancements in subgrade stabilization techniques, including systems for analyzing moisture migration and the dynamic behavior of soils under traffic loads (Wang et al., 2023; Santos et al., 2024). Studies have also explored efficient drainage systems and advanced materials, such as absorbent geotextiles and water-soluble polyurethane, to improve subgrade performance and enhance pavement longevity (Tan et al., 2023; Du et al., 2024; Ma et al., 2024).

Several studies have investigated pavement layers using experimental and numerical methods, with a significant focus on subgrade soil improvement through experimental tests that demonstrate the benefits of additives, fibers, and geosynthetics (Roshan et al., 2022). However, synthetic fibers are more widely used than natural fibers, and conventional stabilizers, such as lime and cement, remain dominant despite the availability of more environmentally friendly alternatives (Gallego-Quintana et al., 2023). However, research on using AC as a stabilizer for subgrade soils remains scarce, representing a gap in the literature. The present study investigates the combined effect of coir fiber, lime, and AC on subgrade stabilization, aiming to enhance the strength and durability of pavement foundations and reduce the amount of conventional stabilizers. Moreover, prior research has extensively demonstrated the adverse effects of cyclic loading on soil subgrades, leading to concerns such as structural degradation and diminished load-bearing capacity (Wang et al., 2020). Many investigations have focused on analyzing the impact of water content, temperature, and weather conditions on subgrade soil performance under traffic loading (Sinha and Iyer, 2020). However, few studies have been conducted on the performance of stabilized and reinforced subgrades under various parameters in numerical investigations, such as the influence of water level on highway pavement performance or the effects of dynamic loading on subgrade layers. Hence, this study seeks to improve the engineering properties of subgrades with natural and recycled additives to model the subgrade performance under various water levels.

Laboratory experiments and FEM analyses were conducted to investigate the performance of the subgrade layers reinforced with coir fiber and stabilized with lime and AC. Initially, laboratory tests, including cyclic CBR, indirect tensile strength (ITS), direct shear (DS), and one-dimensional (1D) consolidation (ODC) tests were conducted to assess the impact of the stabilizers and coir fiber on the subgrade performance. Pavement layers were designed using the American association of state highway and transportation officials (AASHTO) based on experimental data for the subgrade soils. Finally, FEM simulations were performed using ANSYS Workbench. After validation, the effects of the water level and dynamic loading on the performance of the subgrade under varying water levels were predicted, and the allowable strain ratio of the treated subgrade was evaluated using numerical simulations.

2. Material and methods

This study employed two residual soils with different chemical compositions as subgrades. The elemental composition test results, presented in Table 1, indicate that the primary components of both soils were Al_2O_3, SiO_2, and Fe_2O_3, with other oxides present in smaller proportions. Iron (Fe), Aluminum (Al), and Silicon (Si) were the main components. Soils 1 and 2 had silica-alumina ratios (SiO_2/Al_2O_3) of 1.2 and 1.79, respectively, classifying them as real laterites and laterites, according to Martin and Doyne (1927). Additionally, Soil 1 and 2 contained Fe_2O_3 with percentages of 39.44 % and 25.61 %, respectively, which is a significant component of the residual soil (Wahab et al., 2021).

Moreover, the soils were classified based on the AASHTO system (A-7-5). Fig. 1 illustrates the particle size distribution for the two soil types using two analysis methods: the sieve method and laser diffraction. The graph highlights the differences between Soils 1 and 2. Soil 2 contained a higher percentage of coarser particles, while Soil 1 had a greater proportion of finer particles, as evidenced by its steeply rising curve at smaller particle sizes. Hence, Soil 1 had a finer texture, which may contribute to higher cohesion compared to Soil 2. In contrast, Soil 2's coarser texture may result in better drainage properties but lower water retention than Soil 1.

Lime and AC were used as stabilizing materials in the present study. The primary oxides present in lime included CaO (98.85 %), K_2O (0.3 %), SO_3 (0.8 %), and SrO (0.05 %), with particle sizes ranging from 4.79×10^{-4} mm to 0.12 mm. In contrast, AC derived from coconut shell contained 39.77 % CaO, 17.68 % K_2O, 16.62 % P_2O_5, 11.27 % Fe_2O_3, 3.47 % ZnO, 2.57 % MnO, 0.62 % CuO, and 0.18 % SrO, with particle sizes ranging from 8.32×10^{-4} mm to 0.63 mm. Furthermore, coir fiber used as a reinforcer exhibited an average tensile strength of 125 MPa, 1430 kg/m^3 density, and an average diameter of 0.3 mm.

The methodology employed in this study is illustrated in Fig. 2. Initially, the geotechnical properties of the untreated (U) subgrade

Table 1
Soil chemical composition.

Component	Soil 1 (% by mass)	Soil 2 (% by mass)
Fe_2O_3	39.44	25.61
SiO_2	27.69	44.07
Al_2O_3	22.69	24.61
K_2O	5.08	1.55
SO_3	0.53	0.62

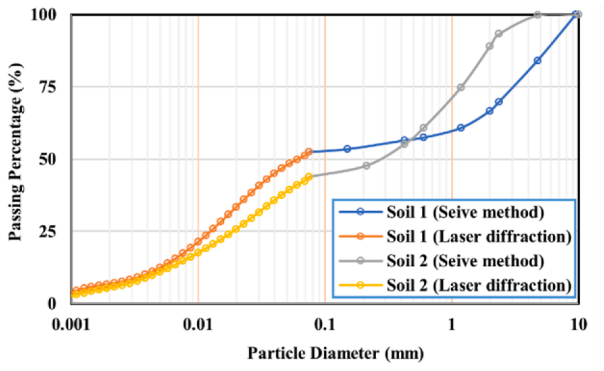

Fig. 1. Particle size analysis of the two residual soil types.

soils were improved using lime (L), AC mixed with coir fiber (ACF), and ACF mixed with lime (ACFL). Various experimental tests were conducted to evaluate the treated soils. Based on the experimental data and the parameters of the other pavement layers listed in Table 2, the pavement layer thickness was determined using the AASHTO method. The modulus of elasticity and density for the same soils were sourced from previous studies (Tamassoki et al., 2023b) and are presented in Table 5. Other mechanical properties were obtained through laboratory testing. These parameters were subsequently utilized to model the pavement layers using the FEM simulation.

3. Experimental methods

3.1. Direct shear test and indirect tensile strength test

This study employed the DS test on all samples to calculate the shear strength parameters based on the British standard 1377: Part 7 (BS 1377, 1990). Three different normal stresses (100 kPa, 200 kPa, and 300 kPa) were applied, with a consistent horizontal displacement rate of 1.25 mm/min was applied. Fig. 3 presents the direct shear device used in this study and the two samples after testing.

In addition, the ITS test was conducted to assess the tensile strength of cylindrical subgrade soil mixtures, each 100 mm in length and 50 mm in diameter. The samples were diametrically loaded between two plates, as shown in Fig. 3. The strength limit of the specimens was determined according to the description outlined in a previous study (Dexter and Kroesbergen, 1985). The testing procedure involved loading the specimens at a rate of 1 mm/min until they reached their peak or failure, which typically resulted in splitting along the loading plane. The ITS value was then calculated using Eq. (1) from (Kamaruddin et al., 2020):

$$ITS = 2P_{ult}/\pi tD \quad (1)$$

where *ITS* represents the tensile strength of the soil specimen, P_{ult} denotes the ultimate load at failure, t is the thickness of the specimen, and D indicates its diameter.

3.2. California bearing ratio test

The CBR values are essential for assessing the bearing capacity and strength of base, subbase, and subgrade course materials used for pavement construction. Although not commonly employed in mechanical design, they are crucial for ensuring the durability and safety of transportation infrastructure. The CBR tests were conducted using compaction methods at the optimum moisture content and maximum dry density. The samples were cured for 28 d in a CBR mold (152 mm inner diameter, 127 mm height) and soaked for 4 d under a 4.5 kg surcharge to replicate the most severe scenario that can arise due to flooding or heavy rainfall on the

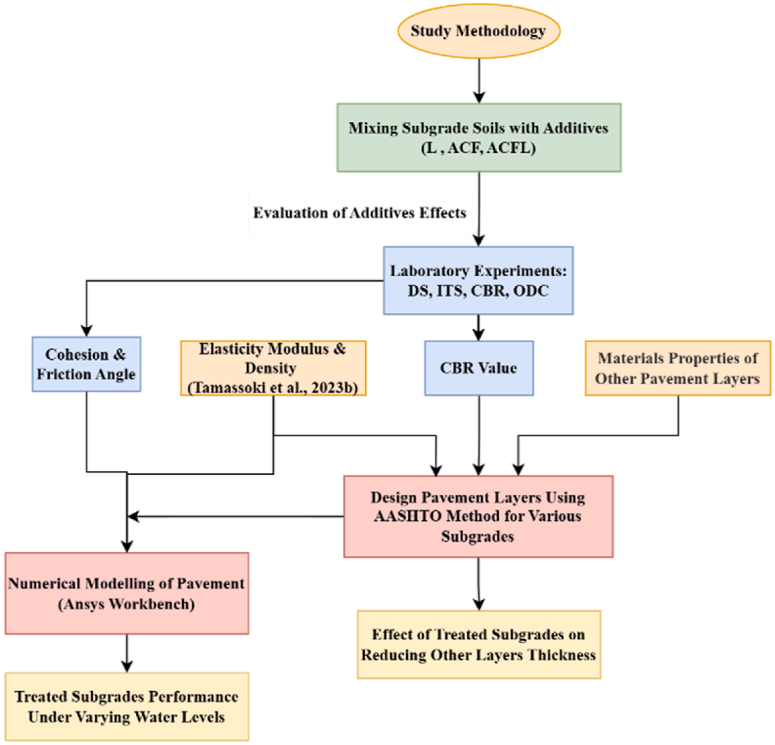

Fig. 2. Methodology process.

Table 2
Properties of materials in other pavement layers.

Layer	Material	CBR (%)	Elastic modulus (MPa)	Poisson's ratio
Wearing surface	Asphalt	–	2744.4	0.45
Base	Granular road base	85	196.5	0.4
Sub-base	Granular sub-base	15	79.29	0.4

subgrade material after construction. Before testing, the samples were drained for 15 min. The CBR value for each specimen was determined by expressing the penetration at 2.5 mm and 5 mm as a ratio relative to the standardized force. Each specimen was subjected to a total penetration of 7.5 mm at a 1 mm/min rate, with readings taken at 0.25 mm intervals. Fig. 4a and b presents lime and the ACFL-treated samples after the CBR test.

3.3. One-dimensional consolidation test

Consolidation settling experiments were conducted following British standard 1377: Part 5 (BS 1377, 1990) to evaluate the permeability of the treated and untreated samples. The specimens were statically compressed into three uniform layers within the consolidation ring (Salimi and Ghorbani, 2020) to achieve the maximum dry density, after which they were cured. Vertical pressures of 50 kPa, 100 kPa, 200 kPa, 400 kPa, and 800 kPa were applied to the samples. Each load increment was maintained for one day to reach 90 % consolidation before recording the final values or applying the next pressure level. The unloading measurements were performed at 200 kPa and 50 kPa. Fig. 4c illustrates the 1D consolidation device that was used in this study.

4. FEM

The FEM was conducted using ANSYS Workbench, which is a widely recognized software for modeling and analyzing complex engineering problems. It is recognized as a robust tool for accurately simulating both linear and nonlinear behaviors and measuring critical responses. The simulation employed the Mohr-Coulomb criterion to model subgrade layers, incorporating key input parameters, including Poisson's ratio, elastic modulus, dynamic load, shear strength parameters, density, and pavement layer thickness.

The simulation involved creating a flexible pavement model consisting of an asphalt surface layered overlying a road subgrade, sub-base, and base materials. The geometry was defined for half of the system, with dimensions of 7 m in width (along the transverse axis) and 25 m in length (along the longitudinal axis). Fig. 5a presents a cross-sectional view of the pavement layers, providing a comprehensive perspective of the simulated finite element analysis.

4.1. Mesh generation

After assigning the material properties, a hexahedral mapped mesh was generated for the FEM, consisting of 28,632 nodes and 4779 elements. Since the mesh structure and density significantly influence the simulation accuracy, an adaptive meshing strategy was employed to achieve an optimal balance between precision and computational efficiency (Xiao et al., 2012). A mesh convergence study was performed to assess the impact of mesh refinement on displacement and stress, ensuring the reliability of the numerical model. As shown in Table 3, reducing the mesh size from 100 mm to 10 mm resulted in only marginal changes in displacement and stress values, confirming that further refinement had a negligible impact on the numerical accuracy. The difference in displacement between the 100 mm and 10 mm meshes was 0.0031 mm, while the corresponding stress difference was 0.22 kPa. This result demonstrates that a finer mesh does not

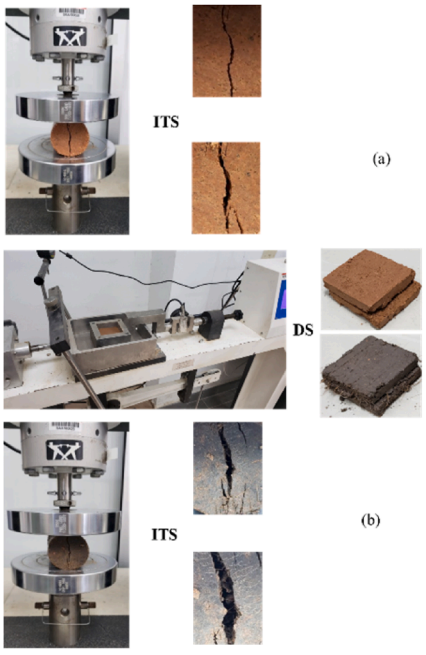

Fig. 3. Direct shear and indirect tensile strength tests: (a) the lime-treated, and (b) the ACF-treated samples.

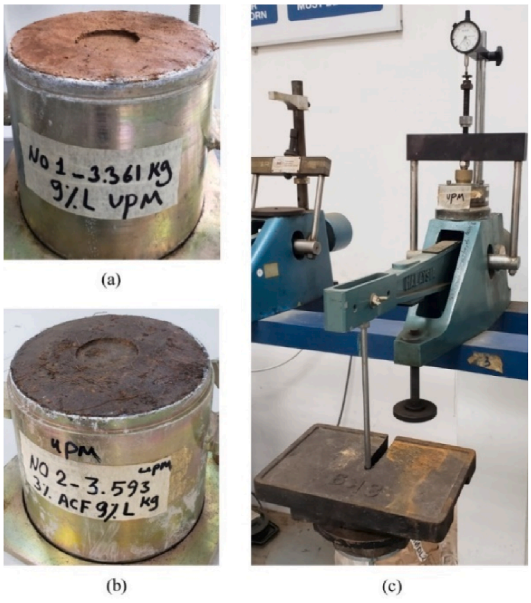

Fig. 4. (a) The lime-treated sample and (b) the ACFL-treated samples after CBR test, and (c) 1D consolidation test.

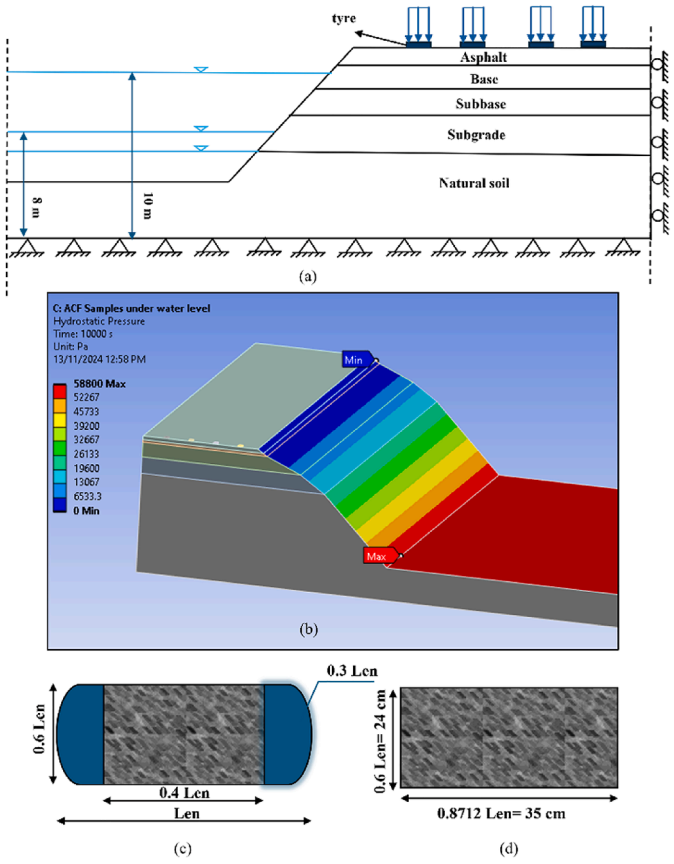

Fig. 5. Details of the modeling and tire contact area: (a) section of model and water levels, (b) hydrostatic pressure for a water level of 8 m, (c) actual tire contact area, and (d) equivalent tire contact area (Length = *Len*).

significantly affect the results beyond a certain threshold, consistent with previous findings on finite element convergence analysis (Yusup et al., 2024). Moreover, computational efficiency remains critical, as excessive mesh refinement increases the processing time without yielding substantial accuracy gains (Mezzadri and Qian, 2022).

Based on Table 3, the analysis reveals that refining the mesh beyond 66.66 mm resulted in negligible changes in displacement (less than 0.00072 mm) and stress (less than 0.052 kPa). Since further refinement to 50 mm or smaller increased the computational cost without significantly improving accuracy, the 50 mm mesh was selected as the optimal size, ensuring an effective balance between numerical precision and computational efficiency.

4.2. Boundary conditions

In this model, roller supports were applied on the sides, restricting the horizontal movement while allowing vertical displacement. The base was fixed to prevent vertical and horizontal movement, ensuring stability and controlled deformation during the simulation. The asphalt surfaces within the model permit vertical displacement to represent pavement behavior realistically under varying loads and conditions.

The interaction modeling approach was employed to simulate the pavement structure, assuming a perfect bond between the pavement layers to minimize sliding and improve accuracy. A frictional interaction between the tires and asphalt was also incorporated, assuming wet asphalt conditions with a friction coefficient of 0.5, as referenced by Singh et al. (2019).

Table 3
Mesh sensitivity analysis for displacement and stress in the FEM.

Mesh size (mm)	Displacement (mm)	Difference	Stress (kPa)	Difference
100	0.3846	–	25.49	–
66.66	0.3856	0.00142	25.56	0.073
50	0.3863	0.00071	25.61	0.051
33.33	0.387	0.00065	25.65	0.042
25	0.3872	0.00023	25.68	0.021
20	0.3874	0.00018	25.69	0.013
16.67	0.3875	0.00013	25.7	0.008
10	0.3877	0.0002	25.71	0.015

4.3. Water pressure simulation

Fig. 5b illustrates the hydrostatic pressure distribution for a water level of 8 m. The hydrostatic pressure was simulated using direct pressure boundary conditions to ensure a realistic representation of the external water forces acting on the subgrade and pavement structure. The hydrostatic pressure distribution was applied according to the depth using the equation $P = \rho gh$, creating a gradual variation in pressure from the water surface to the submerged soil layers.

4.4. Tire contact area and traffic load simulation

Determining the appropriate contact area is essential for accurately assessing deformation under tire loads. The widely adopted method by Nega and Nikraz (2017) calculated the tire contact area using a length of 0.8712*Len* and a width of 0.6*Len*, as depicted in Fig. 5c and d. For a tire load of 40 kN, the contact area consists of two semicircles and a rectangle. Under standard single-axle load conditions of 80 kN, the tire contact area was calculated using a rectangular pressure of 480 kPa, with estimated dimensions of 240 mm in width and 350 mm in length. This approach simplifies the determination of the equivalent contact area for various wheel loads and contact pressures.

The simulation dynamically modeled the traffic load as a moving load. The applied load was precisely defined in terms of the pressure and velocity to replicate real-world pavement conditions accurately. The effect of water level was assessed by applying a cyclic, uniform wheel pressure of 480 kN/m^2 at 60 km/h velocity over the vehicle's wheel contact area.

5. Results and discussion

5.1. Direct shear test

Fig. 6 illustrates the percentage increase in shear strength parameters of treated specimens. The results indicate that ACF enhances both cohesion and friction angle in Soil 2, while in Soil 1, it primarily improves cohesion with a negligible effect on the friction angle. In addition, lime improved the shear strength parameters in both soils. Fig. 6a indicates that adding ACF, L, and ACFL to Soil 1 increases its cohesion by 88.2 %, 106.7 %, and 128.9 %, respectively, whereas for Soil 2, the increases were 4.1 %, 27.6 %, and 155 %, respectively. Similarly, Fig. 6b demonstrates improvements in the friction angle: ACF increased the friction angle by 10.7 % in Soil 2, while the change in Soil 1 was minimal (0.1 %). Lime increased the friction angle by 88 % in Soil 2 and 67.9 % in Soil 1. The more cohesion improvement in Soil 1 with ACF and lime may be attributed to its higher clay content and finer particles, offering a greater surface area for bonding.

In contrast, the coarser particles and lower plasticity of Soil 2 reduce their interactions with stabilizing agents, limiting cohesion

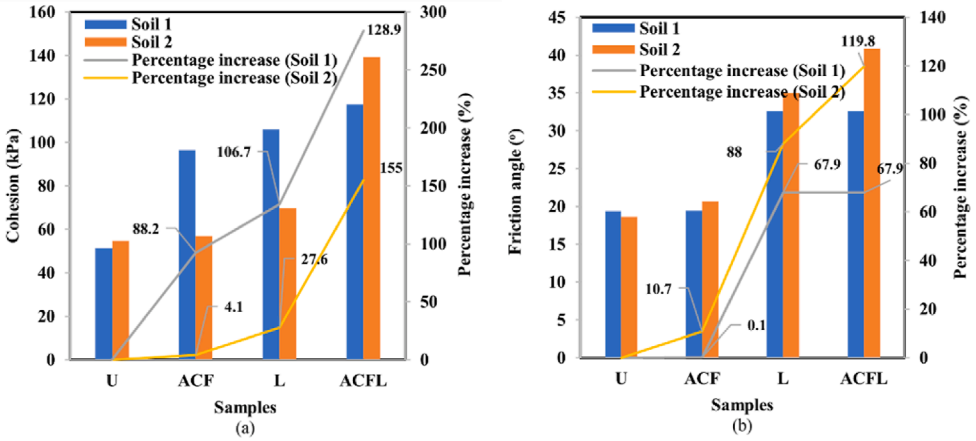

Fig. 6. Improvement of shear strength parameters for two soils with different additives: (a) cohesion, and (b) friction angle.

improvements. However, Soil 2 exhibited a higher friction angle than ACF and the lime-treated Soil 1. Furthermore, ACFL enhanced the friction angle of Soil 2 by 119.8 %, while it did not significantly improve Soil 1 compared to the lime specimen. The addition of ACFL improved the friction angle and cohesion in Soil 2, which benefits more from inter-particle friction and its coarser texture, while Soil 1 responds more effectively to chemical bonding due to its higher clay content and finer particles.

5.2. Indirect tensile test

The ITS test results of the soils treated with ACF, and lime are illustrated in Fig. 7, demonstrating a significant improvement in tensile strength due to the stabilization treatments. The maximum ITS values observed for untreated, ACF, L, and ACFL-treated Soil 1 were 0.34 kPa, 0.65 kPa, 0.85 kPa, and 0.92 kPa, respectively. Similarly, in Soil 2, the maximum tensile strength values for the untreated, ACF, L, and ACFL-treated samples were 0.27 kPa, 1.48 kPa, 6.11 kPa, and 8.45 kPa, respectively. Compared to the untreated samples, the enhancements in the tensile strength of ACF, L, and ACFL-treated Soil 1 were 89.97 %, 149.10 %, and 167.71 %. The improvements for ACF, L, and ACFL-treated Soil 2 were 451.18 %, 2174.96 %, and 3045.86 %, respectively, compared to untreated samples. Including ACF and lime stabilizers in their composition affects the stress-strain behavior and strength of the soils. Specifically, adding stabilizers results in distinct stress-strain behaviors and complementary strengths. Notably, when the predominant tensile zone of the material cracks, specimens that incorporate fiber inclusions continue to have a more significant load and exhibit greater deformation in a ductile manner (Sivakumar Babu et al., 2008; Anggraini et al., 2015).

The maximum tensile strength value increased to 1.12 kN for the ACF sample Soil 1, while the maximum value of 0.65 was considered in the calculation. It should be noted that the observed peak value of 1.12 kPa may be attributed to the fact that the fibers are not typically homogeneous in the specimen, and their orientation during compression may impact the tensile force. Although all mixing was performed manually, and efforts were made to prepare homogeneous mixtures at each mixing instance, variations may occur during testing.

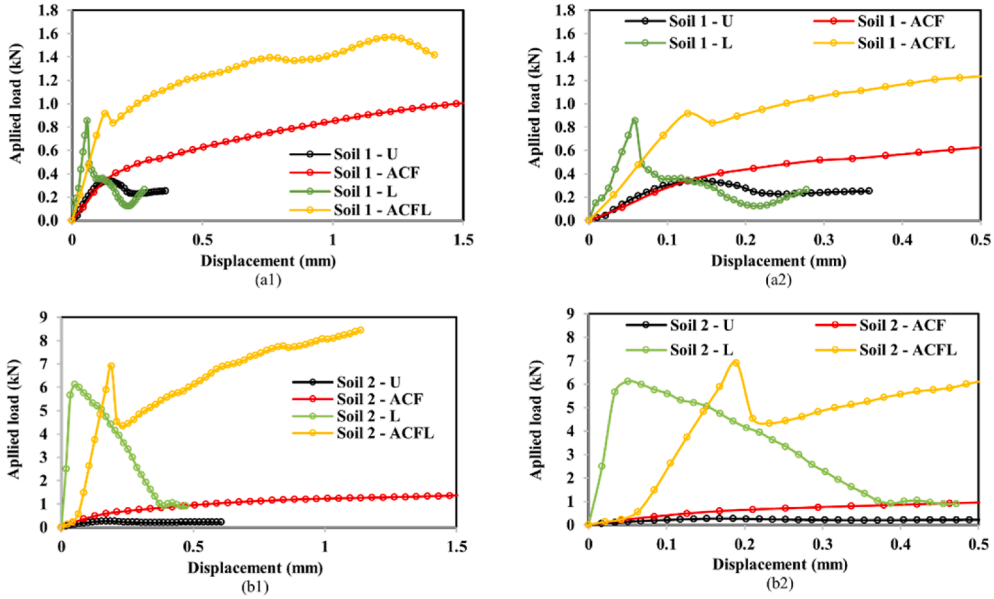

Fig. 7. Load-displacement curves of untreated and treated: (a) Soil 1, and (b) Soil 2.

In particular, the samples treated with lime exhibited brittle behavior, wherein the indirect tensile strength initially increased and then declined sharply. In contrast, the ACF-treated samples displayed flexible behavior compared to the lime-treated samples. Including coir fiber in soil treatment has been observed to improve the indirect tensile strength of the soil. Fatahi et al. (2015) previously reported this phenomenon in their study of cement-treated clay, wherein the inclusion of 0.5 % polypropylene fibers resulted in a similar improvement in tensile strength (Fatahi et al., 2015). Fig. 3 shows the samples obtained after the indirect tensile strength test. It was observed that adding coir fiber to soil samples acted as a bridging element, effectively connecting the soil particles and improving the overall strength of the specimens (Tiwari and Satyam, 2021). Hence, the soil samples treated with ACFL showed improved residual strength compared to those treated with lime. Therefore, it can be inferred that applying ACF to soil enhances its flexibility despite using a higher lime content for stabilization.

5.3. CBR value of soils

The graphical relationship between the load and penetration for the specimens under cyclic loading and soaking conditions is shown in Fig. 8. The findings demonstrate that compared to untreated soils, treatment of both soils with ACF resulted in a slight improvement in CBR values. While Brahmachary and Rokonuzzaman (2018), in their study of natural fiber-reinforced soil, found that adding 1.2 % fiber improved the CBR value of unsoaked and soaked conditions (Brahmachary and Rokonuzzaman, 2018).

The CBR value of the untreated Soil 1 specimen increased from 17.46 % to 23.72 % for the ACF specimen, roughly 1.4 times greater than that of the untreated sample. Similarly, the CBR value of untreated Soil 2 was 14.38 %, which increased to 26.78 % for the ACF sample, approximately 1.9 times that of the untreated sample. Among all the soil mixtures, those containing lime and lime combined with ACF demonstrated the best load-bearing capacity. The CBR of the untreated Soil 1 specimen improved to 84.04 % and 94.69 % for the L and ACFL samples, respectively, roughly 4.8 and 5.4 times greater than that of the untreated sample. Similarly, the CBR value of the untreated Soil 2 increased to 151.52 % and 91.41 % for the L and ACFL samples, respectively, nearly 10.5 and 6.4 times higher than that of the untreated specimen.

The slight increase in the CBR values of ACF in comparison to the lime-treated samples can be attributed to the relatively low percentage of ACF used (2 % and 3 %) compared to lime (9 % and 12 %) (Tamassoki et al., 2022b), as well as the fact that the samples were soaked. Moreover, lime treatment increases soil strength by chemically reacting with soil clay particles to form cementitious compounds, significantly improving the CBR values. However, AC and coir fibers primarily act as reinforcing materials and improve the soil structure through physical means. AC enhances the ability of soil to retain moisture and improves its overall stability, while coir fiber provides mechanical reinforcement and reduces the plasticity of the soil.

Furthermore, dry curing occurs at a higher temperature than under wet or soaked conditions, facilitating water evaporation. This process enhances the interaction between the Si and Al ions and elevates the mixture's pH, leading to greater ion dissolution (Firdous et al., 2018). On the other hand, while Al and Si ions may dissolve under soaked conditions, the excess water keeps them separated, inhibiting or preventing polycondensation and gel formation (Adeyanju et al., 2020).

Fig. 9 illustrates the variations in the maximum penetration for each of the eight soil samples with the number of loading cycles. As expected, the penetration decreased in the treated soil samples and fell with the increasing cycles. However, the penetration rate remained constant for the AC-treated samples, similar to that of untreated soils. Conversely, the penetration rate decreased for the lime and ACFL-treated samples compared to untreated and the ACF samples. Additionally, the penetration rate reduced as cycles increased, starting at 0.9 for untreated Soil 1 to 0.43 and 0.2 for the lime and ACFL-treated samples, respectively. Similarly, the penetration rate declined with the number of cycles, from 0.43 for untreated Soil 2 to 0.25 and 0.2 for the lime and ACFL-treated samples. Mehrpazhouh et al. (2019) reported similar findings when studying the reinforcement of sand with geosynthetics under three repeated loading levels (Mehrpazhouh et al., 2019).

5.4. Effect of additives on permeability

Fig. 10a demonstrates the relationship between void ratio (e) and applied pressure (kPa) for various soil treatments. Both soils follow a similar trend under increasing pressure: the void ratio decreased across all treatments as pressure increases, indicating reduced soil compressibility with increasing load. The untreated soil shows the highest void ratio at each pressure level, whereas the soil treated with the combination of ACF and lime exhibits the lowest void ratio, reflecting the most significant improvement in compressibility. Treatments using only ACF or lime also reduce the

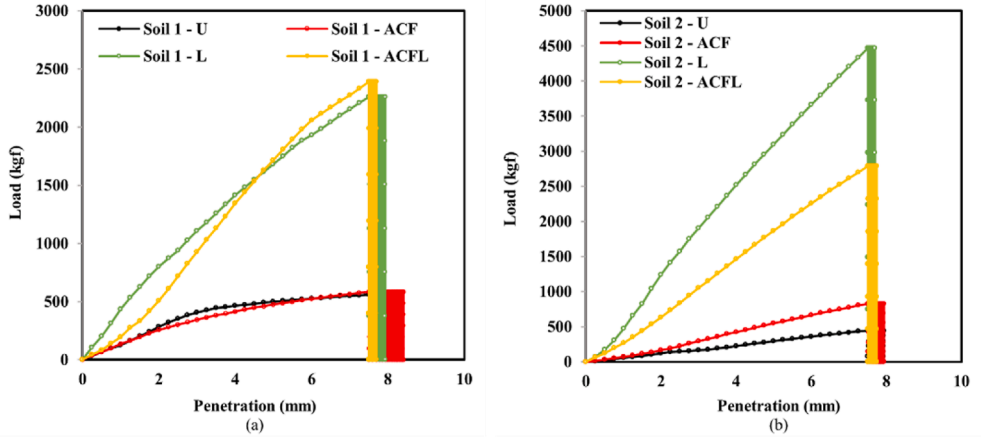

Fig. 8. Load versus penetration curves of samples: (a) Soil 1, and (b) Soil 2 (1 kgf = 9.81 N).

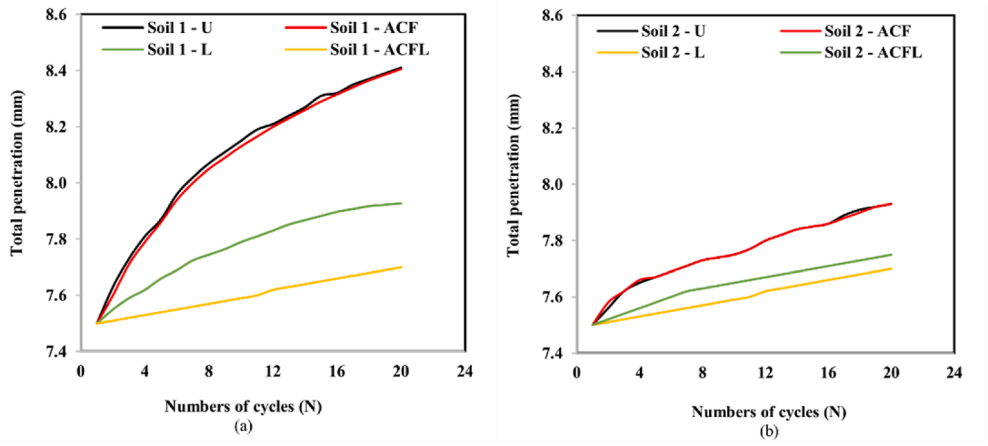

Fig. 9. Relationship between penetration and number of cycles: (a). Soil 1, and (b). Soil 2.

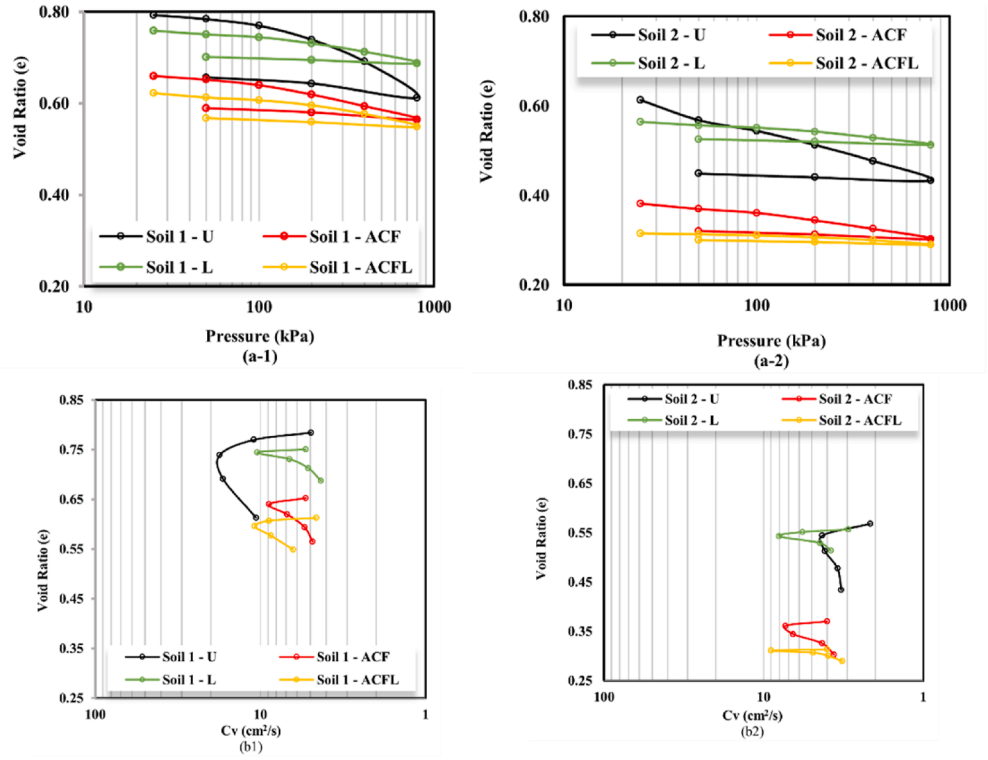

Fig. 10. One-dimensional consolidation: (a) compressibility curves ($e - \log_{10}\sigma'$), and (b) coefficient of consolidation.

void ratio compared to the untreated soils, though not as effectively as the combined treatment. Moreover, the inclusion of AC as an additive further decreases the compressibility of the original soil by filling the voids with its finer particles, as observed by Al-Soudany et al. (2018).

Fig. 10b illustrates the relationship between the void ratio and the coefficient of consolidation (C_v) for both untreated and optimally stabilized soil samples. Stabilized samples exhibit lower void ratios and, consequently, reduced permeability under the same vertical stress compared to the untreated soil. This reduction in the void ratio is attributed to the addition of lime and AC, which decrease the volume of air pockets between soil particles during compaction (Makki-Szymkiewicz et al., 2015). Including ACF further reduced residual soil's porosity, as AC is consists of fine particles with a large surface area (Dillon Jr et al., 1989). Notably, the decrease in C_v values was more pronounced in the lime-treated soils than in AC-treated ones. This is attributed to structural changes in the soil induced by pozzolanic reactions and hydration, which result in a dense and compact matrix. Lower C_v values correspond to reduced soil permeability (Fattah et al., 2014).

Moreover, the permeability coefficient (k) of two soils is shown in Fig. 11. The k values were determined for treated and untreated soil specimens kept saturated in the oedometer cell under varying stress levels. Fig. 11a and b presents the permeability of samples across different stress levels and highlight the effectiveness of lime and AC in reducing soil permeability, an essential factor for drainage in highway construction. Fig. 11c displays the average permeability for each sample. AC decreases permeability by filling

voids and enhancing particle bonding, while lime contributes to further reduction by forming cementation gels during curing, which obstruct water flow (Tamassoki et al., 2022b). Untreated Soils 1 and 2 exhibit higher permeability than the treated samples. Among the treatments, the ACFL-treated soils demonstrate the lowest permeability, indicating a denser structure with fewer voids and gaps.

5.5. Microstructural analysis

Fig. 12 illustrates the microstructural analysis for the ACF and ACFL samples. As shown in Fig. 12a, coir fiber effectively promotes the interconnection of soil particles and reduces the void ratio, leading to a denser and more cohesive structure. The irregular and rough surface morphology of coir fiber facilitates mechanical interlocking between soil particles, increasing frictional resistance and enhancing the bond strength at the fiber-soil interface. Under shear force, soil particles become lodged in the grooves and pores of the fibers, improving the contact area and enabling better stress transfer throughout the matrix. In contrast, synthetic fibers such as polypropylene exhibit smoother surfaces, which lead to lower adhesion with the soil, increased interfacial slip, and a greater likelihood of detachment from the matrix (Raja and Thyagaraj, 2020). This increased fiber-soil interaction in coir-reinforced soil enhanced tensile strength by reinforcing the soil matrix and limiting crack propagation.

Additionally, the void-filling capability of AC plays a crucial role in microstructural refinement by occupying inter-particle spaces, thereby reducing overall porosity. The fine and porous nature of AC facilitates particle rearrangement and densification, improving compressive strength and enhanced load-bearing capacity of the stabilized soil matrix (Hoy et al., 2024). These microstructural changes are directly linked to the observed strength improvements, as confirmed by CBR and tensile strength test results.

Moreover, the presence of Si, Al, and Ca in the lime-treated samples (Table 4) indicates ongoing pozzolanic reactions, leading to the formation of Calcium Silicate Hydrate (CSH) and Calcium Aluminate Hydrate (CAH) gels (see Fig. 12b). These gels function as binding agents, filling voids and promoting matrix densification, which significantly improves soil cohesion and long-term strength (Wahab et al., 2021).

Additionally, AC contributes to soil stabilization by modifying surface properties through its strong adsorption capacity. Its high surface area and porosity allow it to trap organic and inorganic impurities that would otherwise inhibit adequate bonding with stabilizing agents such as lime or cement. AC cleans soil particle surfaces by adsorbing organic matter and immobilizing metal ions and sulfates, which improves soil reactivity with cementitious compounds. The presence of carbon (C) in the ACF-treated sample (Table 4) confirms the precipitation of calcium carbonate ($CaCO_3$), which plays a key role in soil stabilization by filling voids, increasing particle bonding, and reducing permeability. The formation of $CaCO_3$ further improves the mechanical properties of the soil by acting as a cementing agent, enhancing its strength and durability (Crane et al., 2014; Tamassoki et al., 2023b).

5.6. Influence of water level

A high water table near road pavement can significantly impact the roads' structural integrity and durability. When water levels rise close to the pavement, moisture can infiltrate the subgrade and pavement layers, weakening the structural strength and reducing the subgrade's bearing capacity. This moisture intrusion accelerates deterioration through mechanisms such as salt migration and water-induced erosion, ultimately compromising the pavement's ability to support heavy loads over time.

Therefore, stabilizing pavement materials to prevent water ingress and salt movement is critical for maintaining strength performance and extending pavement lifespan. Effective stabilization minimizes the damaging effects of water, ensuring the road remains functional and safe in areas prone to high water levels. Given these concerns, evaluating the impact of water levels is crucial when assessing the stability, particularly for those constructed on clay subgrades, as fluctuations in moisture content can significantly influence the compaction, strength, and overall pavement performance.

FEM is one of the methods employed to evaluate various pavement scenarios. In this study, experimental work conducted

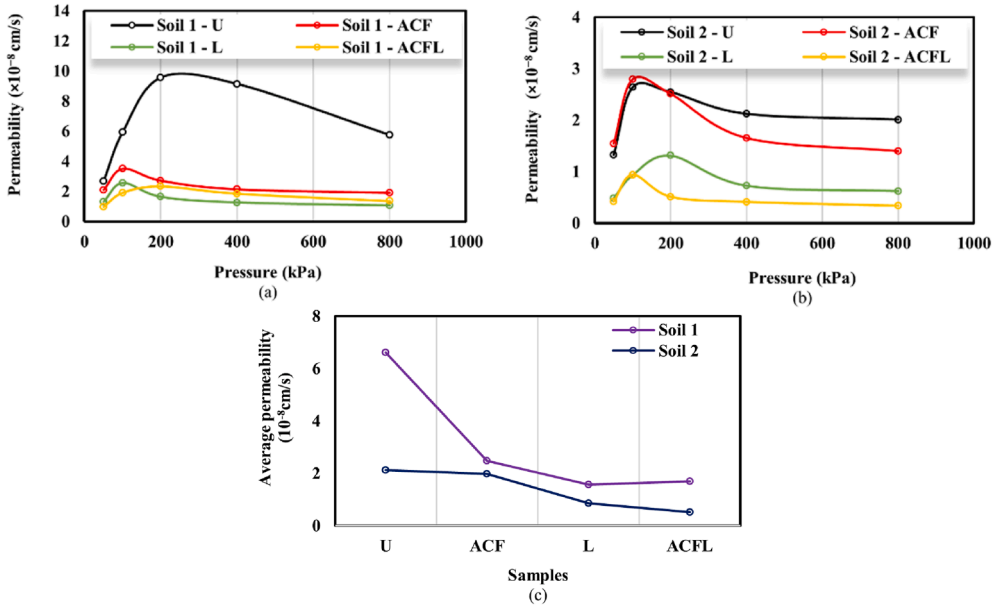

Fig. 11. The permeability value of untreated and treated subgrade: (a) permeability via pressure for Soil 1, (b) permeability via pressure for Soil 2, and (c) average permeability.

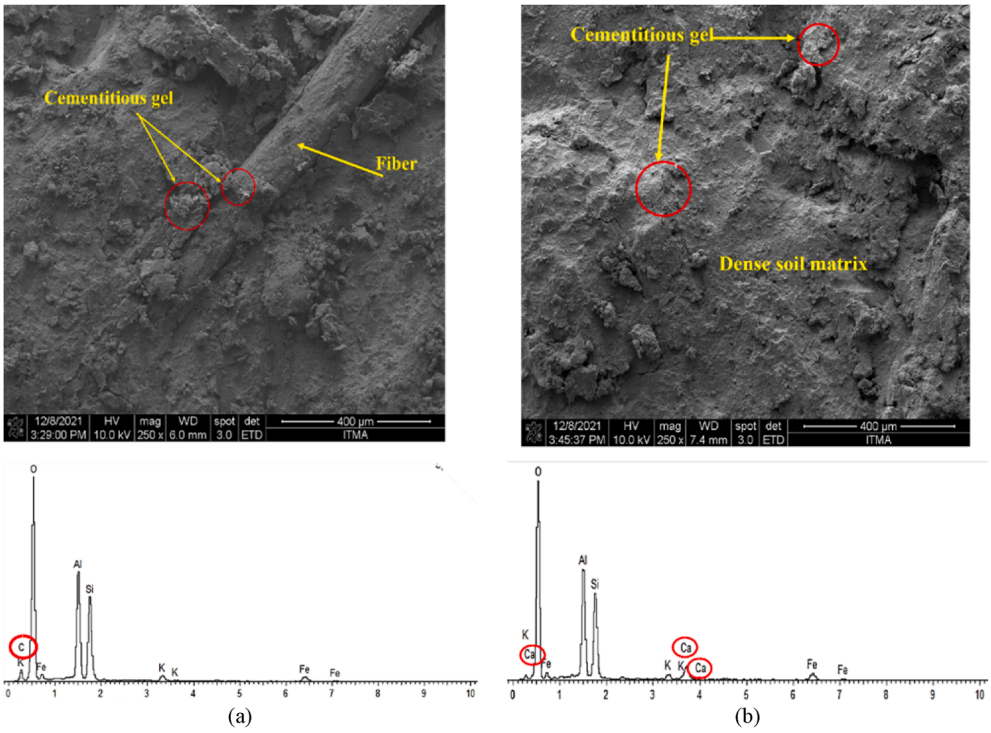

Fig. 12. Field emission scanning electron microscopy micrographs and energy dispersive x-ray spectroscopy, (a) Soil1- ACF, and (b) Soil 2 - ACFL.

Table 4
Elemental composition of Soil 1- ACF and Soil 2 - ACFL.

Sample	Element	O	Al	Si	Fe	K	C	Ca
Soil 1- ACF	Weight (%)	58.36	14.74	13.64	5.35	1.45	6.46	–
	Atomic (%)	68.18	10.21	9.08	1.79	0.69	10.06	–
Soil 2 - ACFL	Weight (%)	58.83	14.54	13.93	7.16	1.41	–	4.14
	Atomic (%)	73.85	10.82	9.96	2.58	0.72	–	2.07

by Tang et al. (2016) was first replicated to validate the FEM model. Fig. 13a illustrates the vertical stress response and subgrade resilient deformation obtained from the experimental model, while Fig. 13b presents these parameters for the FEM model. The vertical stresses exerted on the subgrade by the wheel load in the numerical model are approximately 25 kPa, closely aligning with the experimental model reported by Tang et al. (2016) and the full-scale pavement data presented by Al-Qadi et al. (2012). These findings suggest that the stress conditions simulated for the subgrade soil in this study represent those observed in real-world full-scale accelerated pavement testing and confirm the model's accuracy in replicating previous experimental findings.

In addition, Fig. 14 illustrates permanent deformation and more loading cycles from experimental and numerical modeling under a single tire pressure. The numerical results closely align with the experimental findings, particularly after 4000 cycles. However, some discrepancies are observed during the early stages of cyclic loading. These differences are attributed to the limitations of the numerical model in modeling early-stage strain accumulation in clay subgrades, and potential experimental uncertainties. In pavement applications, the initial few thousand load cycles typically induce rapid plastic strain accumulation before stabilization, a behavior that Mohr-Coulomb-based models do not fully replicate. Previous studies have highlighted, that early-stage plasticity, including cyclic plastic strain accumulation and rutting behavior, is challenging to simulate without advanced material models or shakedown-based approaches (Xiao et al., 2018a; Pérez-González et al., 2023).

Additionally, stress-path-dependent cyclic plastic strain energy and permanent deformation mechanisms in cohesive soils remain challenging to model accurately without advanced constitutive frameworks or bounding surface plasticity models (Cai et al., 2018; Xiao et al., 2018b). Experimental uncertainties, such as sensor drift, initial seating effects, and variations in soil compaction, may also contribute to deviations in early-cycle results (Gluchowski et al., 2023). Despite these challenges, numerical and experimental results demonstrate improved agreement over time, indicating that

Table 5
The thickness of the sub-base layer (D3) according to various subgrades.

Subgrade samples	Soil 1 -U	Soil 1 -ACF	Soil 1 -L	Soil 1 -ACFL	Soil 2 -U	Soil 2 -ACF	Soil 2 -L	Soil 2 -ACFL
Maximum dry density (g/cm^3)	1.53	1.62	1.52	1.57	1.6	1.68	1.59	1.64
Optimum moisture content (%)	21.5	22.6	23.6	23.9	16.2	17.4	20.75	21.2
Cohesion (kPa)	51.29	96.52	106.01	117.38	54.59	56.81	69.68	139.2
Friction angle (°)	19.41	19.42	31.25	32.58	18.62	20.62	35	40.92
Elastic modulus (kPa)	9071.01	18538.23	52986.4	66150.66	5890.25	11292.3	41601.41	64926
Sub-base calculated based on subgrade (D_3) (cm)	140	89	25.4	15.5	198	132	41	18
Percentage reduction D_3 (%)	–	36.43	81.86	88.93	–	33.33	79.29	90.91

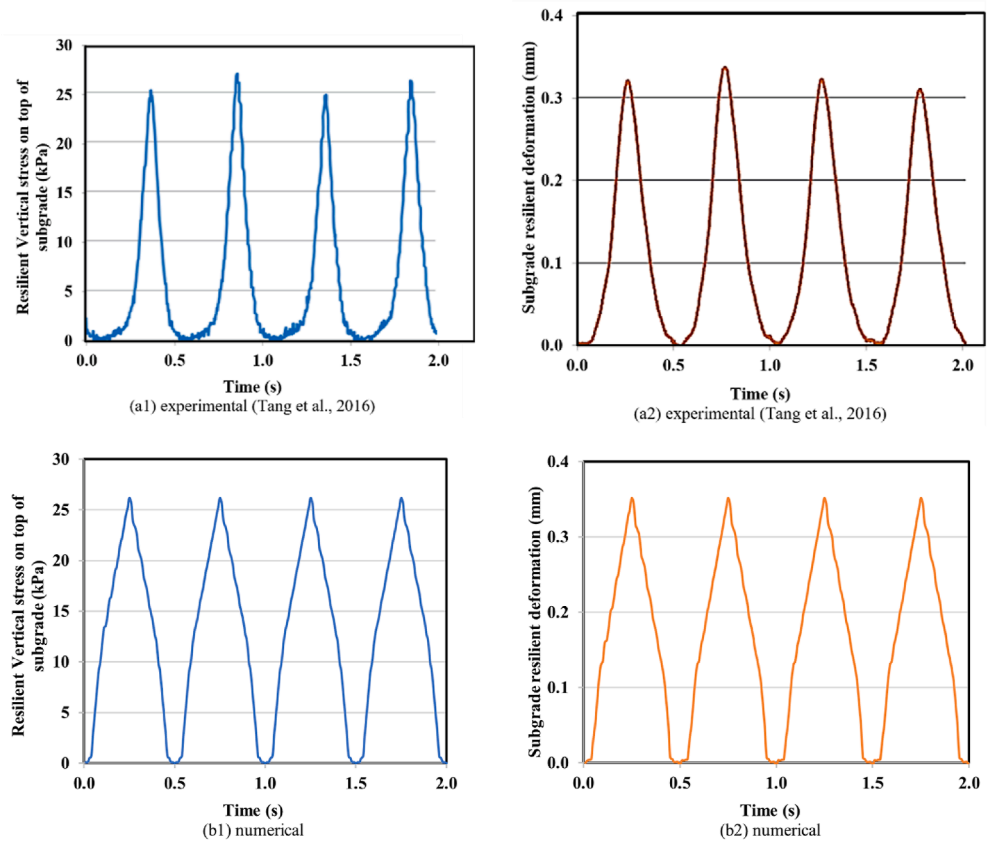

Fig. 13. Subgrade settlement patterns and resilient vertical of subgrade: (a) experimental model (Tang et al., 2016), and (b) numerical model.

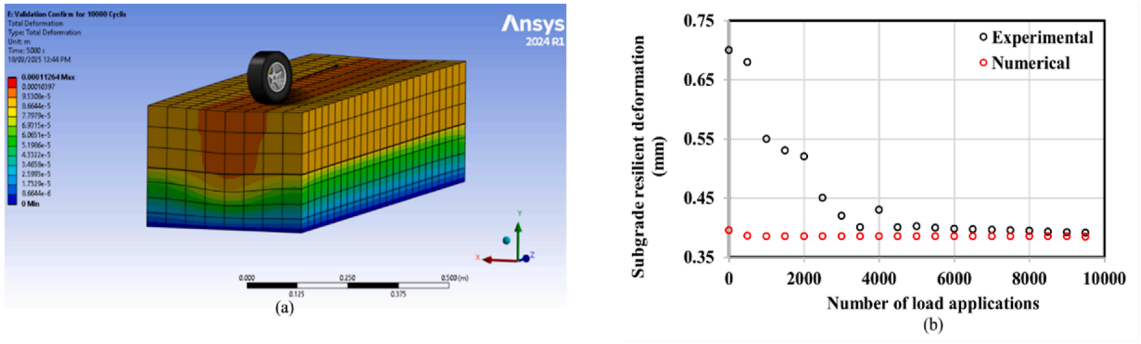

Fig. 14. Subgrade total deformation under various load cycles: (a) numerical model, and (b) comparison of experimental and numerical deformation results.

the model reasonably captures the long-term deformation trends in clay subgrades.

The model was refined and adjusted to better align with the new dataset, enabling the assessment of stabilized subgrade soil performance under varying water levels and aligning with the research objectives. The proposed project involves the construction of a new four-lane highway, with each lane measuring 3.5 m in width. Traffic distribution is expected to consist of 20 % in the fast lane and 80 % in the slow lane. The highway is designed to accommodate an equivalent single-axle load (ESAL) of 16.85 million standard axles (Msa) over its service life. A traffic growth factor 23.28 has been applied to account for expected traffic increases over time. The design ensures a reliability level of 90 %, with a standard deviation of 0.4 to account for variability in performance predictions. The initial serviceability index (PSI) is 4.2, with a terminal PSI 2. Based on this information, along with data from the experimental phase and Table 2, the pavement layer thickness was determined using the AASHTO design method, considering both untreated and treated subgrade conditions. The pavement structure comprises four layers: asphalt, base, sub-base, and subgrade, with a 0.23 m asphalt layer (D_1), a 0.155 m base layer (D_2), and a 2 m subgrade layer (D_4). The sub-base thickness (D3) was determined based on the subgrade properties, resulting in eight design variations, along with other parameters used in the FEM analysis, all of which are presented in Table 5.

The inclusion of additives significantly influences the required subbase thickness for both soil types. For Soil 1, the subbase thickness decreased by 88.93 % from 140 cm for untreated Soil 1 to 15.5 cm when treated with ACFL. Similarly, in Soil 2, the subbase thickness was reduced by 90.91 % from 198 cm for the untreated

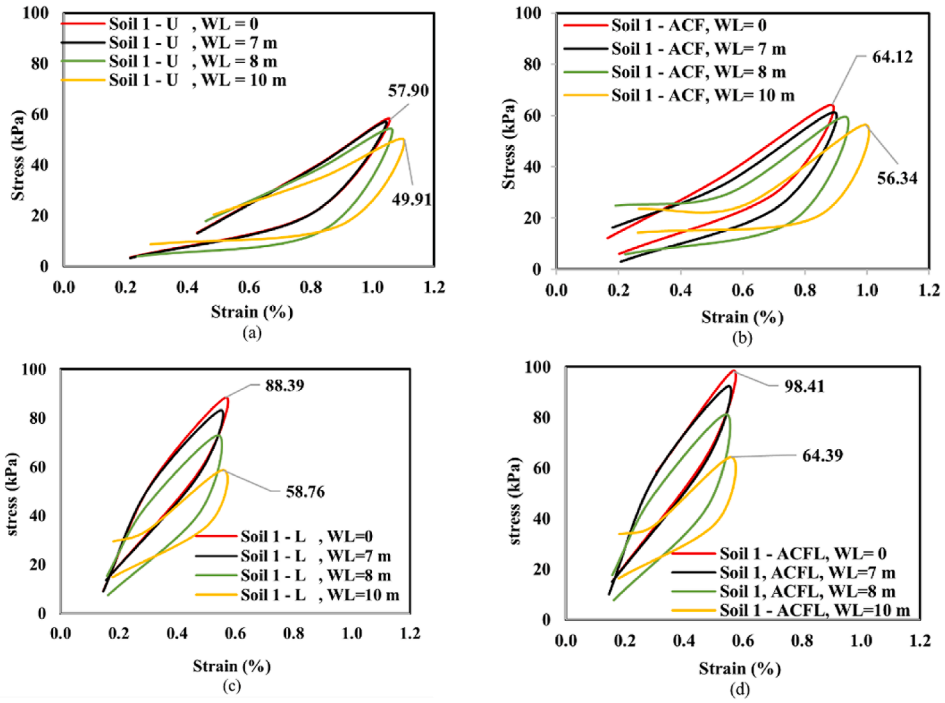

Fig. 15. Stress-strain curves of subgrade Soil 1: (a) untreated, (b) the ACF-treated, (c) the lime-treated, and (d) the ACFL-treated samples.

Soil 2 to 18 cm with the addition of ACFL. These results demonstrated the effectiveness of the additives in enhancing soil strength and minimizing subbase thickness requirements.

Fig. 15 presents the relationship between stress and strain for a single cycle to better illustrate the effect of water levels. When the water level was at 10 m, the peak value of the stress-strain curve decreased, indicating that higher water levels reduced the soil's strength. This reduction in strength with increasing water levels is attributed to several factors. Elevated water levels increase pore water pressure, which reduces the effective stress that holds soil particles together, thereby weakening the soil structure (Elshaer and Daniel, 2018). Additionally, higher moisture content

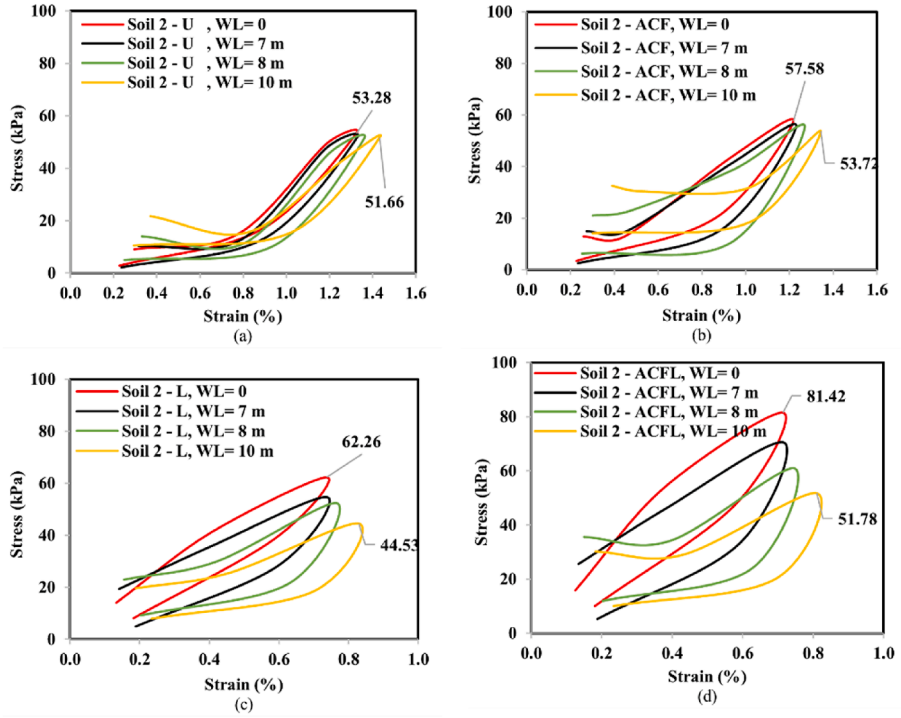

Fig. 16. Stress-Strain curves of subgrade Soil 2: (a) untreated, (b) the ACF-treated, (c) the lime-treated, and (d) the ACFL-treated samples.

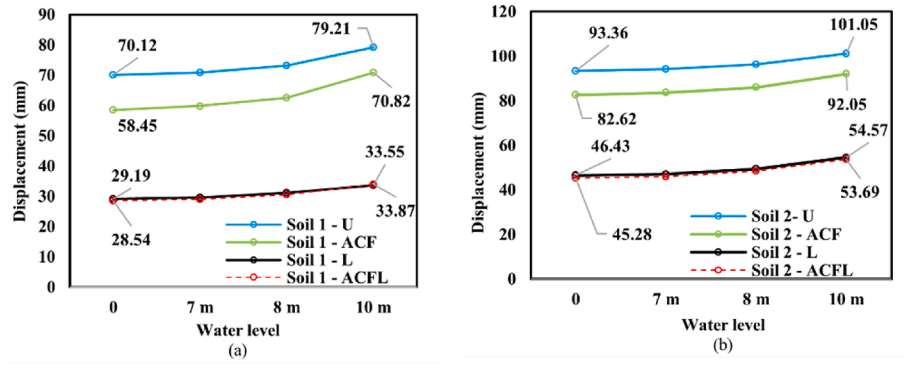

Fig. 17. Settlement - water level of untreated and treated subgrade: (a) Soil 1, and (b) Soil 2.

decreases cohesion between soil particles, particularly in clay-rich soils, and increases pore water pressure, diminishing inter-particle friction and shear strength (Huo et al., 2021). Soil saturation also leads to a loss of capillary action and suction, further reducing shear strength. Moreover, water acts as a lubricant, facilitating particle movement and lowering the soil's resistance to shear forces (Indraratna et al., 2020).

The data indicate that the stress-strain curves decrease as the water level increases, demonstrating a negative impact where higher water levels lead to greater strain and displacement. For instance, the peak stress for untreated subgrade Soil 1 decreased from 57.90 kPa to 49.91 kPa under dry conditions at a 10 m water level. Similarly, the peak stress for the ACF-treated subgrade decreased from 64.12 kPa to 56.34 kPa. The lime-treated and ACFL subgrades' peak stress declined from 88.39 kPa to 58.76 kPa and 98.41 kPa to 64.39 kPa, respectively.

Moreover, Fig. 16 illustrates the impact of water levels on the stress-strain curves for the untreated, ACF, L, and ACFL samples of Soil 2. The results indicate that increasing water levels significantly affect the peak stress–strain values. Under dry conditions, the peak stress-strain for the untreated subgrade was 53.28 kPa, which decreased to 51.66 kPa at a 10 m water level. Likewise, the peak stress-strain values for ACF, lime, and ACFL subgrades decreased from 57.58 kPa to 53.72 kPa and 62.29 kPa to 44.53 kPa and 81.42 kPa to 51.78 kPa, respectively, under the same water levels.

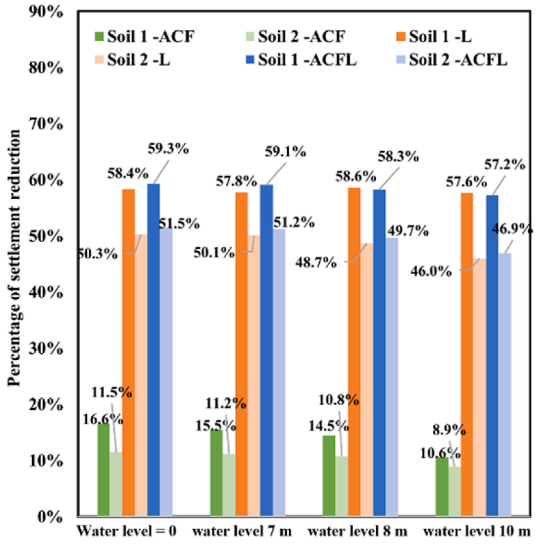

Fig. 18. Percentage reduction in settlement for treated samples compared to untreated soils.

Fig. 17 shows that the untreated subgrade exhibited more displacement at all water levels than the treated subgrades. For the treated subgrade Soil 1 (Fig. 17a), the settlement decreased from 70.12 mm for untreated Soil 1 to 58.45 mm for ACF, 29.19 mm for lime, and 28.54 mm for ACFL under dry conditions. A similar trend is observed at other water levels. For example, at a 10 m water level, the settlement reduced from 79.21 mm for the untreated subgrade to 70.82 mm for ACF, 33.55 mm for lime, and 33.87 mm for the ACFL-treated subgrade.

Similarly, Fig. 17b indicates that settlements increased with rising water levels for treated and untreated subgrade Soil 2. Moreover, the results demonstrate that the untreated subgrade experienced greater settlement than the others, whereas the ACFL subgrade exhibited the least settlement. The maximum settlement is 101.05 mm, which belongs to the untreated subgrade at a 10 m water level, in contrast to the minimum settlement of 45.28 mm, which occurred in the ACFL-treated subgrade under dry conditions.

Fig. 18 indicates the percentage reduction in settlement for treated soil samples compared to untreated soils. The data reveals a notable decrease in settlement across all treated samples relative to the untreated soils. Specifically, the lime and the ACFL treatments significantly reduced settlement compared to the ACF treatment. For Soil 1, the ACF sample showed settlement reduction ranging from 10.6 % to 16.6 %, while the L and the ACFL treatments consistently maintained higher settlement reduction values around 58 % to 59 %. Similarly, for Soil 2, the ACF samples exhibited settlement reduction from 8.9 % to 11.5 %, whereas the L and ACFL treatments demonstrated superior performance, maintaining settlement reduction between 46 % and 51.5 %. These results indicate that lime and the ACFL treatments are more effective in reducing settlement than ACF, highlighting their potential for improving soil stability.

5.7. Strain ratio

The criteria for subgrade strain outlined by AUSTROADS (2004a), as given in Eq. (2), can be reformulated to show that (Gribble and Patrick, 2005):

$$\varepsilon = 9.3 \times 10^{-3}\, N^{-1/7} \tag{2}$$

where ε (expressed in strain units) represents the maximum design strain permissible for a total design traffic loading of N. According to Eq. (2), the maximum allowable subgrade strain is 0.0086 for traffic volumes of 16.85×10^6 ESAL. The following graphs in Fig. 19 show the subgrade strain ratio according to the

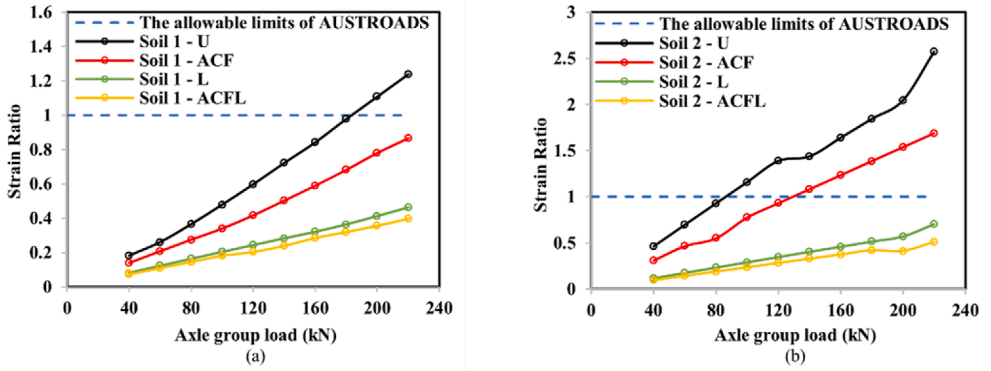

Fig. 19. Strain ratio of subgrade samples: (a) Soil 1, and (b) Soil 2.

maximum allowable strain. The strain ratio is defined as the strain at the top of the subgrade divided by the allowable strain specified by AUSTROADS for the proposed traffic (Gribble and Patrick, 2005). When the strain ratio is less than 1, the strain is within the allowable limit. According to Fig. 19, the ACF, lime, and ACFL treatments for subgrade Soil 1 all fall within the allowable standard due to the soil's finer texture, which enhances reactivity and binding with stabilizing agents. In contrast, for subgrade Soil 2, which is coarser, the stabilization provided by ACF alone is insufficient, as the reduced fine particle content limits its effectiveness. However, the lime and ACFL treatments successfully improve Soil 2 by enhancing particle cohesion and interlocking, allowing them to meet the requirements for pavement design.

6. Conclusions

This study conducted numerical and experimental analyses to evaluate the flexible pavement subgrade stability using AC, lime, and coir fiber. The results confirmed that incorporating ACFL enhanced the engineering properties of both Soil 1 and Soil 2. In Soil 1, the ACFL treatment increased cohesion from 51.29 kPa to 117.38 kPa, friction angle from 19.41° to 32.58°, and indirect tensile strength from 0.34 kPa to 0.92 kPa, reducing the required subbase thickness by 89 %. Similar trends were observed in Soil 2, where ACFL improved cohesion from 54.59 kPa to 139.20 kPa and friction angle from 18.62° to 40.92°, cutting the subbase thickness by approximately 91 %.

Notably, the synergistic effect of AC, lime, and coir fiber resulted in settlement reduction of 59.3 % and 51.5 % for Soils 1 and 2, respectively, compared to untreated soils. Untreated soils demonstrated substantial settlement across all water levels due to their high permeability and poor geotechnical properties, making them susceptible to volume changes and deformation under traffic loading. In contrast, the ACFL-treated samples exhibited superior stability with reduced displacement, attributed to their higher elastic modulus, friction angle, cohesion, and lower permeability, ensuring greater resistance to cyclic loading effects.

Stress-strain analyses further revealed that ACFL displayed lower strain while withstanding higher stress, confirming its effectiveness in enhancing subgrade strength. The ACF and the lime-treated samples displayed intermediate settlement, stress, and strain characteristics, positioning them between untreated and the ACFL-stabilized soils in terms of performance. Additionally, strain ratio analysis confirmed that the ACFL and L samples in both soil types and the ACF-treated sample in Soil 1 meet the criteria for subgrade materials, validating the effectiveness of these stabilization methods for flexible pavement applications.

CRediT authorship contribution statement

Sakina Tamassoki: Writing – review & editing, Writing – original draft, Visualization, Validation, Software, Resources, Project administration, Methodology, Investigation, Funding acquisition, Formal analysis, Data curation, Conceptualization. **Shanyong Wang:** Writing – review & editing, Visualization, Validation, Supervision, Software, Resources, Project administration, Methodology, Investigation, Funding acquisition, Formal analysis, Data curation, Conceptualization. **Nik Norsyahariati Nik Daud:** Writing – review & editing, Visualization, Validation, Supervision, Software, Resources, Project administration, Methodology, Investigation, Funding acquisition, Formal analysis, Data curation, Conceptualization. **Mohammad Jawed Roshan:** Writing – review & editing, Visualization, Validation, Software, Methodology, Investigation, Funding acquisition, Formal analysis, Data curation, Conceptualization.

Declaration of competing interest

The authors declare that they have no known competing financial interests or personal relationships that could have appeared to influence the work reported in this paper.

Acknowledgments

The authors are very grateful to the University of Newcastle and Universiti Putra Malaysia for their partial support of the study presented in this paper, which is supported by the ARC Discovery Project grants (Grant Nos. DP210100437 and DP230100126) and ARC Linkage Project (LP230201048).

References

Abdi, M.M.R., Ghalandarzadeh, A., Chafi, L.S., 2021. An investigation into the effects of lime on compressive and shear strength characteristics of fiber-reinforced clays. J. Rock Mech. Geotech. Eng. 13 (4), 885–898.

Adeyanju, E., Okeke, C.A., Akinwumi, I., Busari, A., 2020. Subgrade stabilization using rice husk Ash-based geopolymer (GRHA) and Cement Kiln Dust (CKD). Case Stud. Constr. Mater. 13, e00388.

Al-Qadi, I.L., Tutumluer, E., Dessouky, S., 2012. Construction and instrumentation of full-scale geogrid-reinforced flexible pavement test sections. In: Xiao, T., Sun, J., Wang, X., Chen, Z. (Eds.), Geotech. Spec. Publ., No. 212. ASCE, Reston, VA, pp. 131–142.

Al-Soudany, K., Al-Gharbawi, A., Al-Noori, M., 2018. Improvement of clayey soil characteristics by using activated carbon. In: MATEC Web Conf., 162, 01009.

Amakye, S.Y.O., Abbey, S.J., Booth, C.A., 2022. Road pavement defect investigation using treated and untreated expansive road subgrade materials with varying plasticity index. Transport Eng. 9, 100123.

Anggraini, V., Asadi, A., Huat, B.B.K., Nahazanan, H., 2015. Effects of coir fibers on tensile and compressive strength of lime treated soft soil. Meas. 59, 372–381.

Arivalagan, J., Indraratna, B., Rujikiatkamjorn, C., Warwick, A., 2022. Effectiveness

of a Geocomposite-PVD system in preventing subgrade instability and fluidization under cyclic loading. Geotext. Geomembr. 50 (4), 607–617.
Behnood, A., 2018. Soil and clay stabilization with calcium- and non-calcium-based additives: a state-of-the-art review of challenges, approaches and techniques. Transp. Geotech. 17, 14–32.
Boobalan, S.C., Sivakami Devi, M., 2022. Investigational study on the influence of lime and coir fiber in the stabilization of expansive soil. Mater. Today Proc. 60, 311–314.
Brahmachary, T.K., Rokonuzzaman, M., 2018. Investigation of random inclusion of bamboo fiber on ordinary soil and its effect CBR value. Int. J. Geo-Eng. 9, 1–11.
BS 1377, 1990. Methods of Test for Soils for Civil Engineering Purposes.
Cai, Y., Chen, Y., Cao, Z., Ren, C., 2018. A combined method to predict the long-term settlements of roads on soft soil under cyclic traffic loadings. Acta Geotech 13, 1215–1226.
Chen, X., Zhang, J., Wang, X., 2015. Full-scale field testing on a highway composite pavement dynamic responses. Transp. Geotech. 4, 13–27.
Correia, A.G., Roshan, M.J., 2024. Self-sensing cementitious geocomposites in rail track substructures. Transp. Geotech. 46, 101260.
Crane, R.E., Cassidy, D.P., Srivastava, V.J., 2014. Activated carbon preconditioning to reduce contaminant leaching in cement-based stabilization of soils. J. Environ. Eng. 140 (10), 04014032-2–04014032-7.
Dexter, A.R., Kroesbergen, B., 1985. Methodology for determination of tensile strength of soil aggregates. J. Agric. Eng. Res. 31 (2), 139–147.
Dillon Jr, E.C., Wilton, J.H., Barlow, J.C., Watson, W.A., 1989. Large surface area activated charcoal and the inhibition of aspirin absorption. Ann. Emerg. Med. 18 (5), 547–552.
Du, Y., Cui, X., Hao, J., Li, X., Bao, Z., Zhang, S., et al., 2024. Investigation of three-dimensional dynamic response and work area depth in heavy-haul railway subgrade based on a theoretical model. Transp. Geotech. 45, 101219.
Elshaer, M., Daniel, J.S., 2018. Impact of pavement layer properties on the structural performance of inundated flexible pavements. Transp. Geotech. 16, 11–20.
El-Shafey, E.I., Ali, S.N.F., Al-Busafi, S., Al-Lawati, H.A.J., 2016. Preparation and characterization of surface functionalized activated carbons from date palm leaflets and application for methylene blue removal. J. Environ. Chem. Eng. 4 (3), 2713–2724.
Farhangi, V., Moradi, M.J., Daneshvar, K., Hajiloo, H., 2024. Application of artificial intelligence in predicting the residual mechanical properties of fiber reinforced concrete (FRC) after high temperatures. Constr. Build. Mater. 411, 134609.
Fatahi, B., Khabbaz, H., Fatahi, B., 2015. Mechanical characteristics of soft clay treated with fibre and cement. Geosynth. Int. 19 (3), 252–262.
Fattah, M.Y., Al-saidi, A., Jebur, M.M., 2014. Consolidation properties of compacted soft soil stabilized with lime-silica fume mix. Int. J. Sci. Eng. Res. 5 (7), 1675–1682.
Firdous, R., Stephan, D., Yankwa Djobo, J.N., 2018. Natural pozzolan based geopolymers: a review on mechanical, microstructural and durability characteristics. Constr. Build. Mater. 190, 1251–1263.
Gallego-Quintana, P., Ojeda-Farias, O.F., Alvarez-Rosario, A., Alvarez-Sánchez, E.J., Landa-Ruiz, L., Terán-Torres, B.T., Mendoza-Rangel, J.M., Baltazar-Zamora, M.A., 2023. Analysis of the mechanical properties of a stabilized subgrade type soil under a sustainable approach for construction. Materials 16 (19), 6395.
Gluchowski, A., Zając, K., Sas, W., 2023. Evaluating the long-term plastic strain accumulation in reclaimed asphalt pavement (RAP) application for road subbase construction: a cyclic triaxial loading study. In: IOP Conf. Ser.: Mater. Sci. Eng., 1297, 012013.
Gribble, M., Patrick, J., 2005. Adaptation of the AUSTROADS pavement design guide for New Zealand conditions. Land Transport New Zealand Res. Rep. 305, 42.
Hoy, M., Tran, N.Q., Suddeepong, A., Horpibulsuk, S., Mobkrathok, M., Chinkulkijniwat, A., Arulrajah, A., 2023. Improved fatigue properties of cement-stabilized recycled materials – lateritic soil using natural rubber latex for sustainable pavement applications. Transp. Geotech. 40, 100959.
Hoy, M., Horpibulsuk, S., Chinkulkijniwat, A., Suddeepong, A., Buritatum, A., Yaowarat, T., Choenklang, P., Udomchai, A., Kantatham, K., 2024. Innovations in recycled construction materials: paving the way towards sustainable road infrastructure. Front. Built Environ. 10, 1–10.
Huo, W., Zhang, W., Zhu, Z., Peng, Y., 2021. Experimental and numerical simulation study on mechanical and engineering properties of silt roadbed under capillary water. Bull. Eng. Geol. Environ. 80, 8211–8229.
Indraratna, B., Singh, M., Nguyen, T.T., Leroueil, S., Abeywickrama, A., Kelly, R., Neville, T., 2020. Laboratory study on subgrade fluidization under undrained cyclic triaxial loading. Can. Geotech. J. 57 (11), 1767–1779.
Jairaj, C., Prathap Kumar, M.T., Ramesh, H.N.H., Kumar, M., Ramesh, H.N.H., 2020. Effect of addition of lime on coir fiber admixed BC soil. Innov. Infrastruct. Solut. 5.
Kamaruddin, F.A., Nahazanan, H., Kim Huat, B., Anggraini, V., 2020. Improvement of marine clay soil using lime and alkaline activation stabilized with inclusion of treated coir fibre. Appl. Sci. 10, 2129.
Lee, C.S., Ong, Y.L., Aroua, M.K., Daud, W.M.A.W., 2013. Impregnation of palm shell-based activated carbon with sterically hindered amines for CO_2 adsorption. Chem. Eng. J. 219, 558–564.
Li, X., Yang, Y., Wang, J., Yu, Q., Yu, H., 2022. Deformation of pavement subgrade subjected to traffic loads considering multi-direction principal stress rotation. Soil Dynam. Earthq. Eng. 162, 107480.
Ma, C., Feng, H., Wang, C., Zhang, N., Liu, Y., Li, J., Liu, X., Li, S., Jiang, H., Li, Y., 2024. A numerical simulation of moisture reduction in fine soil subgrade with wicking geotextiles. Materials 17 (2), 390.
Makki-Szymkiewicz, L., Hibouche, A., Taibi, S., Herrier, G., Lesueur, D., Fleureau, J.M., 2015. Evolution of the properties of lime-treated silty soil in a small experimental embankment. Eng. Geol. 191, 8–22.
Martin, F.J., Doyne, H.C., 1927. Laterite and lateritic soils in Sierra Leone. J. Agric. Sci. 17 (4), 530–547.
Mehrpazhouh, A., Moghadas Tafreshi, S.N., Mirzababaei, M., 2019. Impact of repeated loading on mechanical response of a reinforced sand. J. Rock Mech. Geotech. Eng. 11 (4), 804–814.
Mezzadri, F., Qian, X., 2022. Density gradient-based adaptive refinement of analysis mesh for efficient multiresolution topology optimization. Int. J. Numer. Methods Eng. 123 (2), 465–504.
Narendra Goud, G., Hyma, A., Shiva Chandra, V., Sandhya Rani, R., 2018. Expansive soil stabilization with coir waste and lime for flexible pavement subgrade. In: IOP Conf. Ser: Mater. Sci. Eng., 330, 012130.
Nega, A., Nikraz, H., 2017. Evaluation of tire-pavement contact stress distribution of pavement response and some effects on the flexible pavements. In: Proc. Int. Conf. Highway Pavements and Airfield Technol, pp. 174–185, 2017.
Pérez-González, E.L., Bilodeau, J.-P., Doré, G., 2023. Plastic strain rate in granular materials as a function of stress history: a probabilistic approach for the PBD model. Int. J. Pavement Eng. 24 (2), 1–12.
Praveen, G.V., Kurre, P., 2021. Influence of coir fiber reinforcement on shear strength parameters of cement modified marginal soil mixed with fly ash. Mater. Today Proc. 39, 504–507.
Raja, P.S.K., Thyagaraj, T., 2020. Sulfate effects on sulfate-resistant cement–treated expansive soil. Bull. Eng. Geol. Environ. 79, 2367–2380.
Razali, R., Rashid, A.S.A., Che Lat, D., Horpibulsuk, S., Roshan, M.J., Rahman, N.S.A., et al., 2023. Shear strength and durability against wetting and drying cycles of lime-stabilized laterite soil as subgrade. Phys. Chem. Earth, Parts A/B/C 132, 103479.
Roshan, M.J., Safuan A Rashid, A., Abdul Wahab, N., Tamassoki, S., Norafida Jusoh, S., Azril Hezmi, M., et al., 2022. Improved methods to prevent railway embankment failure and subgrade degradation: a review. Transp. Geotech. 37, 100834.
Roshan, M.J., Abedi, M., Gomes Correia, A., Fangueiro, R., Mendes, P.M., 2024. A multifunctional cementitious composite for pavement subgrade. Materials 17 (3), 621.
Salimi, M., Ghorbani, A., 2020. Mechanical and compressibility characteristics of a soft clay stabilized by slag-based mixtures and geopolymers. Appl. Clay Sci. 184, 105390.
Santos, T.A.d., Pinheiro, R.J.B., Specht, L.P., 2024. Effects of moisture content and soil suction on the permanent deformation of tropical subgrade soils: experimental investigations and modelling. Road Mater. Pavement Des. 25 (11), 2358–2381.
Shojaeifard, M., Baghani, M., Shahsavari, H., 2020. Rutting investigation of asphalt pavement subjected to moving cyclic loads: an implicit viscoelastic–viscoplastic–viscodamage FE framework. Int. J. Pavement Eng. 21 (11), 1393–1407.
Singh, D., Patel, H., Habal, A., Das, A.K., Kapgate, B.P., Rajkumar, K., 2019. Evolution of coefficient of friction between tire and pavement under wet conditions using surface free energy technique. Constr. Build. Mater. 204, 105–112.
Sinha, P., Iyer, K.K.R., 2020. Effect of stabilization on characteristics of subgrade soil: a review. In: Advances in Computer Methods and Geomechanics, Lecture Notes in Civil Engineering, pp. 667–682.
Sivakumar Babu, G.L., Vasudevan, A.K., Sayida, M.K., 2008. Use of coir fibers for improving the engineering properties of expansive soils. J. Nat. Fibers 5 (1), 61–75.
Tamassoki, S., Nik Daud, N.N., Jakarni, F.M., Kusin, F.M., Rashid, A.S.A., Roshan, M.J., 2022a. Compressive and shear strengths of coir fibre reinforced activated carbon stabilised lateritic soil. Sustainability 14 (15), 9100.
Tamassoki, S., Nik Daud, N.N., Jakarni, F.M., Kusin, F.M., Rashid, A.S.A., Roshan, M.J., 2022b. Performance evaluation of lateritic subgrade soil treated with lime and coir fibre-activated carbon. Appl. Sci. 12 (16), 8279.
Tamassoki, S., Nik Daud, N.N., Nejabi, M.N., Roshan, M.J., 2023a. Fibre-reinforced soil mixed lime/cement additives: a review. Pertanika J. Sci. & Technol. 31 (1), 217–235.
Tamassoki, S., Nik Daud, N.N., Wang, S., Roshan, M.J., 2023b. CBR of stabilized and reinforced residual soils using experimental, numerical, and machine-learning approaches. Transp. Geotech. 42, 101080.
Tan, P., Wang, F., Guo, C., Liu, J., 2023. Cyclic stress–strain characteristics of red clay treated with permeable water-soluble polyurethane. Transp. Geotech. 42, 101072.
Tang, X., Palomino, A.M., Stoffels, S.M., 2016. Permanent deformation behaviour of reinforced flexible pavements built on soft soil subgrade. Road Mater. Pavement Des. 17 (2), 311–327.
Tiwari, N., Satyam, N., 2020. An experimental study on the behavior of lime and silica fume treated coir geotextile reinforced expansive soil subgrade. Eng. Sci. Technol. Int. J. 23 (5), 1214–1222.
Tiwari, N., Satyam, N., 2021. Coupling effect of pond ash and polypropylene fiber on strength and durability of expansive soil subgrades: an integrated experimental and machine learning approach. J. Rock Mech. Geotech. Eng. 13 (5), 1101–1112.
Tiwari, N., Satyam, N., Puppala, A.J., 2021. Strength and durability assessment of expansive soil stabilized with recycled ash and natural fibers. Transp. Geotech. 29, 100556.
Wahab, N.A., Roshan, M.J., Rashid, A.S.A., Hezmi, M.A., Jusoh, S.N., Nik

Norsyahariati, N.D., Tamassoki, S., 2021. Strength and durability of cement-treated lateritic soil. Sustainability 13 (11), 6430.
Wang, S., Li, X., Ren, K., Liu, C., 2020. Experimental research on steel slag stabilized soil and its application in subgrade engineering. Geotech. Geol. Eng. 38, 4603–4615.
Wang, L., Zhang, L., Wang, T., Zhang, S., 2023. Investigation of water and soil migration and mud pumping of subgrades under traffic load. Atmosphere 14 (1), 133.
Xiao, T., Sun, J., Wang, X., Chen, Z., 2012. Dynamic response analysis of cement concrete pavement under different vehicle speeds. Pavements and Materials: Recent Advances in Design, Testing and Construction. Geotechnical Special Publication No. 212. ASCE, p. 128.
Xiao, Y., Zheng, K., Chen, L., Mao, J., 2018a. Shakedown analysis of cyclic plastic deformation characteristics of unbound granular materials under moving wheel loads. Constr. Build. Mater. 167, 457–472.
Xiao, Y., Zhang, Z., Chen, L., Zhang, K., 2018b. Modeling stress path dependency of cyclic plastic strain accumulation of unbound granular materials under moving wheel loads. Mater. Des. 137, 9–12.
Yusup, E.M., Azahari, H., Saiful, S., Mansor, F., Mat, M.N.H., Jabbar, B.A., 2024. A mesh convergence study for 2D axisymmetric pipe wall thickness. J. Adv. Res. Micro Nano Eng. 23 (1), 77–90.

Dr. Shanyong Wang is a Professor at the School of Engineering at the University of Newcastle, Australia. His excellent research reputation is built upon his development of novel computer codes and advanced engineering testing, and his expertise actively bridges the gap between academic and industrial practice. He won the ARC Future Fellowship in 2014. He was awarded the 2018 John Booker Medal in Engineering Science by the Australian Academy of Science. Since 2002, He has published 318 refereed journal articles and conference papers. Also, he is an associate editor of the Canadian Geotechnical Journal and an Editorial Board member for 10 top international SCI journals such as Engineering Geology, Canadian Geotechnical Journal, Computers and Geotechnics, Rock Mechanics and Rock Engineering, Journal of Rock Mechanics and Geotechnical Engineering, Acta Geotechnica, Transportation Geomechanics. He is a fellow of Engineers Australia (FIEAust) and a member of the American Society of Civil Engineers (ASCE).